Thin-Walled Structures 86 (2015) 132–141

Contents lists available at ScienceDirect

Thin-Walled Structures

journal homepage: www.elsevier.com/locate/tws

Analytical simulation of nonlinear elastic–plastic average stress–average strain relationships for un-corroded/both-sides randomly corroded steel plates under uniaxial compression

Mohammad Reza Khedmati *, Zorareh Hadj Mohammad Esmaeil Nouri

Department of Marine Technology, Amirkabir University of Technology, Tehran 15914, Iran

ARTICLE INFO

Article history:
Received 26 August 2012
Received in revised form
14 October 2014
Accepted 14 October 2014
Available online 6 November 2014

Keywords:
Imperfect steel plate
Both-sides random corrosion
Ultimate strength
Average stress–average strain relationship
Simulation

ABSTRACT

In this paper, an analytical simplified method for derivation of the average stress–average strain relationship of imperfect steel plates taking into account of both geometric and material nonlinearities is presented. The method utilizes the theory of elastic large deflection analysis of plates in the elastic region, and also the theory of rigid-perfectly plastic mechanism analysis of plates in the plastic region. The ultimate strength of the plate is predicted using an empirical formulation. The steel plates may be entirely un-corroded or both-sides randomly corroded. The algorithm can be easily implemented in methods for evaluation of ship hull girder ultimate strength as well as in the estimation of the ultimate capacity of offshore structures.

1. Introduction

In design of ships and offshore structures, it is essential to ensure that the structure has sufficient strength to sustain extreme loading situations. Such marine structures are mostly assembled of plates and plated elements. Thus, strength of plates and other plated elements is crucial for the overall structural capacity or in other words for the ultimate strength of the whole structure. For a thorough assessment of a structural design, for understanding possible improvements and to predict the consequences in the event of failure, an approximation of the value of ultimate strength is not sufficient. The complete behaviour, up to collapse and beyond, of the structure has to be simulated to gain insight into causes and effects of a structural failure.

For the analysis of large marine structures, an accurate and efficient approach is required to obtain results within a reasonable space of the time. Despite the enormous development in computer technology, elastic-plastic large deflection analyses with conventional finite element analysis (FEA) are too time-consuming for large structures. Therefore, a simplified method has to be employed to reduce the computational time and/or increase the size of the structural parts that can be analysed.

For cross sections of ships in bending, methods to obtain the moment-curvature relationship, Fig. 1, considering the collapse of parts of the cross section have been developed. One of the most known methods is the Smith's method [1,2], in which the ship cross-section is divided into small elements each of which is composed of plates without/with stiffener. Average stress–average strain relationships of all elements are derived before the analysis of the whole cross-section progresses as follows: curvature is applied incrementally about the instantaneous neutral axis, the strain of each element is calculated, the corresponding stress is taken from the stress–strain curves previously derived, and the corresponding moments is obtained by integration over the cross-section, Fig. 2. FEA is usually applied in order to derive the average stress–average strain relationships of plate and stiffened plate elements. Application of FEA in derivation of average stress–average strain relationships of the plated elements in the cross-section of a ship hull girder or any other box-shape structure would mean spending a considerable amount of cost and time. Therefore, it is felt that there is a need to develop or propose a simplified method in order to perform such calculations. These calculations create a significant step in progressive collapse analysis of marine structures.

Analytical method proposed in this paper, is one suitable framework for implementing a general approach to collapse analysis, since it leads to the reduction of solution process either in time or in cost. Combining the theory of elastic large deflection analysis with rigid-plastic mechanism analysis, a simple formulation is expressed in order to derive average stress–average strain relationships of plates. The accuracy of the method or formulation is verified against the FEA obtained results. Employing such a formulation, the ultimate strength

* Corresponding author. Tel.: +98 21 64543113; fax: +98 21 66412495.
E-mail address: khedmati@aut.ac.ir (M. Reza Khedmati).

http://dx.doi.org/10.1016/j.tws.2014.10.012
0263-8231/

Notations

AR	aspect ratio of the plate
a	plate length
b	plate breadth
t	thickness of plate in un-corroded condition
t_{eq}	effective thickness of plate in corroded condition
t_P	thickness function of plate in un-corroded condition
E	Young modulus of material
ν	Poisson's ratio of material
m	number of half-waves in longitudinal direction
m_0, m_{45}, m_{90}	some constants in the rigid-plastic mechanism analysis relationships
n	number of half-waves in transverse direction
β	plate slenderness
F	Airy's stress function
μ	mean corrosion depth
S	standard deviation of random thickness variations
n_y	number of years of exposure
d_w	uniform reduction in thickness
r_1, r_2	random numbers corresponding to the corroded surfaces of the plate
z_{UpSRF}	Z-coordinate of the upper surface of the plate
z_{LowSRF}	Z-coordinate of the lower surface of the plate
U_x	displacement along x-axis
U_y	displacement along y-axis
U_z	displacement along z-axis
A_{0ij}	coefficients in initial deflection function
w_0	initial deflection function
$w_{0\ max}$	maximum magnitude of initial deflection
w_e	elastic deflection
w_p	plastic deflection
ε	strain
ε_Y	material yield strain
σ	stress
σ_Y	material yield stress
σ_U	material ultimate stress
σ_{Ult}	ultimate compressive strength of the plate
$r,\ r-1$	rth and $(r-1)$th values of the parameter

evaluation of ships and offshore structures is possible in a very short time with reasonable accuracy and cost.

2. General assumptions

The longitudinal stiffening system is usually employed in large ships at their mid-length part, especially in the deck and bottom structures. If an extreme bending moment acts on a hull girder, the most possible collapse mode may be the overall collapse of stiffened panel after local collapse of individual plate elements between stiffeners.

The following assumptions are made in the derivation of the average stress–average strain relationships of the plate elements:

1. Attached plating between longitudinal stiffeners behaves as an isolated plate.
2. The material is assumed to be elastic-perfectly plastic.

Average stress–average strain relationships of the isolated plates are derived combining the results of elastic large deflection analysis and rigid plastic mechanism analysis.

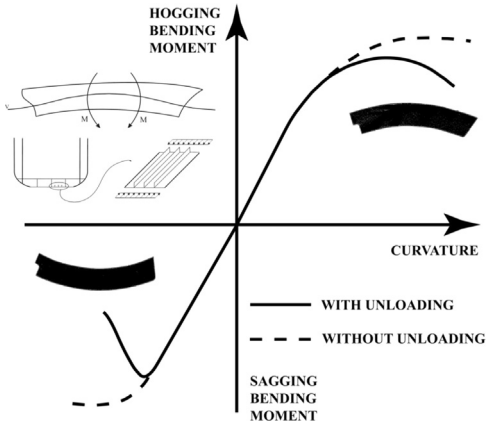

Fig. 1. Typical moment–curvature relationship.

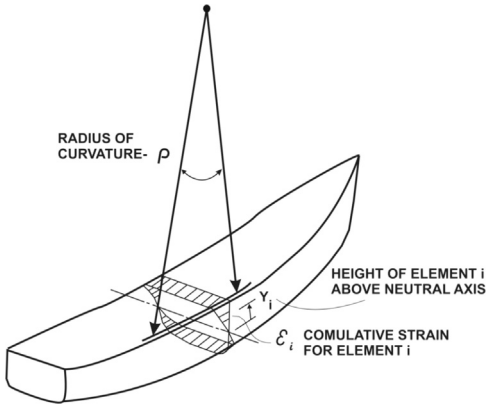

Fig. 2. Ship hull girder bending concept (Smith's method).

3. Average stress–average strain relationship of un-corroded plates

3.1. Welding induced initial deflections

In a thin-walled plated structure, the initial deflection of a local plate panel is produced by the fillet welding between plate and stiffeners. The resulting typical shape of initial deflection is the so-called *thin-horse mode* that deflects in the same direction in adjacent spans or bays. An example of initial deflection of the inner-bottom plating of an existing Handy-sized Bulk Carrier, measured by Yao et al. [3], is illustrated in Fig. 3. As shown, the rectangular plate panels have an almost symmetric mode of initial deflection across the bays and spans. The usual assumption of asymmetric modes of initial deflection based on the linear elastic

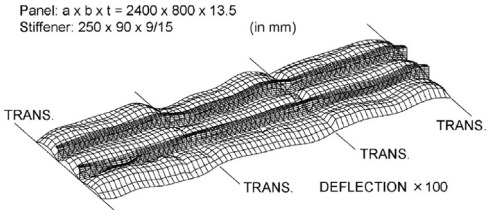

Fig. 3. Real distribution of initial deflection or so-called thin-horse mode initial deflection [3].

buckling analysis gives very conservative predictions of the ultimate strength [4].

Theoretically, for a plate of length a, breadth b, and thickness t, the initial deflection of a thin-horse mode can be expressed by a double sinusoidal series as

$$w_0 = \sum_{i=1}^{\infty}\sum_{j=1}^{\infty} A_{0ij} \sin\frac{i\pi x}{a}\sin\frac{j\pi y}{b} \tag{1}$$

Among the deflection components in the direction of the shorter side of the plate (y-direction), the first term with one half-wave has the greatest effect on the initial deflection mode. Thus, a simpler form of the initial deflection equation can be written as follows

$$w_0 = \sum_{i=1}^{\infty} A_{0i} \sin\frac{i\pi x}{a}\sin\frac{\pi y}{b} \tag{2}$$

Ueda and Yao [5] idealised this mode with another expression as follows which includes only odd terms

$$w_0 = \sum_{i=1,3,5,\ldots}^{21} A_{0i} \sin\frac{i\pi x}{a}\sin\frac{\pi y}{b} \tag{3}$$

Later Yao et al. [6], introduced even terms also in this mode, and finally the idealised thin-horse mode of initial deflection took the following form

$$w_0 = \sum_{i=1}^{11} A_{0i} \sin\frac{i\pi x}{a}\sin\frac{\pi y}{b} \tag{4}$$

The initial deflection is herein assumed to be in the idealised thin-horse mode. The coefficients of this mode (A_{0i}), nondimensionalised by plate thickness (t), i.e., A_{0i}/t, are given in Table 1 [6] as functions of plate aspect ratio.

In Fig. 4, the maximum initial deflection measured in Japanese shipyards [5] is plotted against β^2t, where β is the slenderness parameter of the plate defined by

$$\beta = \frac{b}{t}\sqrt{\frac{\sigma_Y}{E}} \tag{5}$$

σ_Y and E are the yield stress and Young's modulus, respectively. Smith et al. [7] have categorized their measured data of maximum initial deflection by statistical analysis into three levels, "slight", "average" and "severe", and formulated equations as shown in Fig. 4. "slight" and "severe" correspond to 3% and 97% fractals of probability distribution function, respectively. On the other hand, Japanese Ship Quality Standard (JSQS) prescribes an upper limit of 6 mm for the maximum allowable initial deflection. It can be seen from Fig. 4 that the measured data are distributed such that the "average" line and the allowable limit prescribed by JSQS form an upper bound. Taking average level of the measured maximum deflection in Fig. 4, the maximum magnitude of initial deflection, w_{0max}, is taken as

$$w_{0\,max} = 0.05\beta^2 t \tag{6}$$

To consider the plate continuity, it is assumed that the plate is simply-supported along its four edges which remain straight while subjected to in-plane movements.

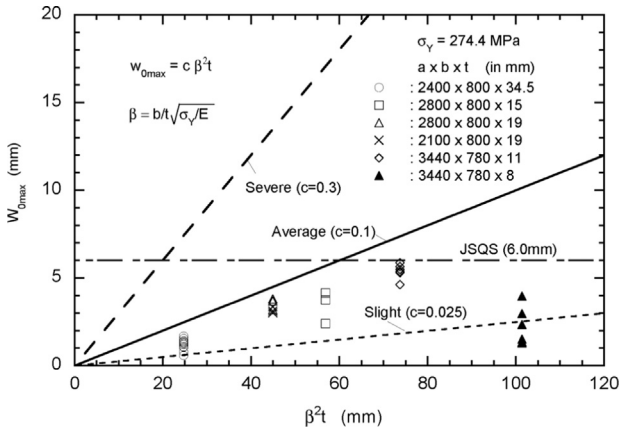

Fig. 4. Maximum initial deflections of rectangular plates measured in ships [5].

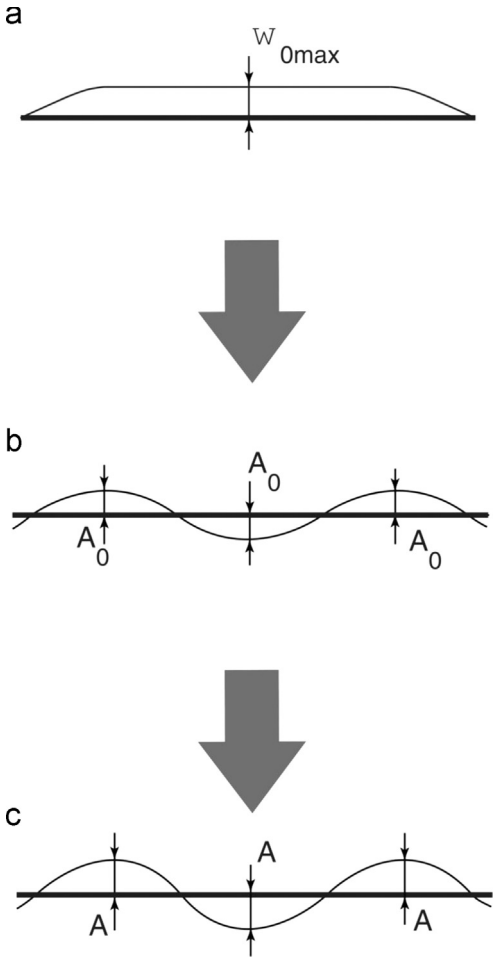

Fig. 5. Changes in deflection mode and its magnitude. (a) Idealised thin-horse mode initial deflection. (b) Equivalent stable mode initial deflection. (c) Final deflection mode after applying in-plane compression.

Table 1
Coefficients of thin-horse mode initial deflection as a function of plate aspect ratio [6].

a/b	A_{01}/t	A_{02}/t	A_{03}/t	A_{04}/t	A_{05}/t	A_{06}/t	A_{07}/t	A_{08}/t	A_{09}/t	A_{010}/t	A_{011}/t
$1 < a/b < \sqrt{2}$	1.1158	−0.0276	0.1377	0.0025	−0.0123	−0.0009	−0.0043	0.0008	0.0039	−0.0002	−0.0011
$\sqrt{2} < a/b < \sqrt{6}$	1.1421	−0.0457	0.2284	0.0065	0.0326	−0.0022	−0.0109	0.001	−0.0049	−0.0005	0.0027
$\sqrt{6} < a/b < \sqrt{12}$	1.1458	−0.0616	0.3079	0.0229	0.1146	−0.0065	0.0327	0.000	0.000	−0.0015	−0.0074
$\sqrt{12} < a/b < \sqrt{20}$	1.1439	−0.0677	0.3385	0.0316	0.1579	−0.0149	0.0743	0.0059	0.0293	−0.0012	0.0062
$\sqrt{20} < a/b < \sqrt{30}$	1.1271	−0.0697	0.3483	0.0375	0.1787	−0.0199	0.0995	0.0107	0.0537	−0.0051	0.0256

The total deflection mode under the action of in-plane longitudinal compression is assumed to follow as:

$$w = \sum_{i=1}^{11} A_i \sin\frac{i\pi x}{a} \sin\frac{\pi y}{b} \tag{7}$$

3.2. Stable mode

With the increase of the compressive load above the buckling load, just one single deflection component among the deflection components A_i is magnified [6]. Consequently, taking single deflection modes as follows can approximate the behaviour of the plate

$$w_0 = A_{0m} \sin\frac{m\pi x}{a} \sin\frac{\pi y}{b} \tag{8}$$

and

$$w = A_m \sin\frac{m\pi x}{a} \sin\frac{\pi y}{b} \tag{9}$$

In above equations, m is the number of half-waves in the stable deflection mode above the plate buckling load, and is determined as [6]

$$m = \begin{cases} 1 : a/b < 1.3 \\ k : k-0.7 \le a/b < k+0.3 \end{cases} \tag{10}$$

where a/b is the plate aspect ratio and k is an integer greater than 1. Hereafter, A_{0m} and A_m are simply denoted as A_0 and A, respectively. Fig. 5 exhibits changes in the deflection mode of the plate from beginning to the end of simulations.

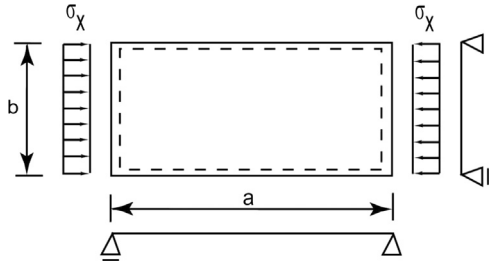

Fig. 6. Rectangular plate under longitudinal compression.

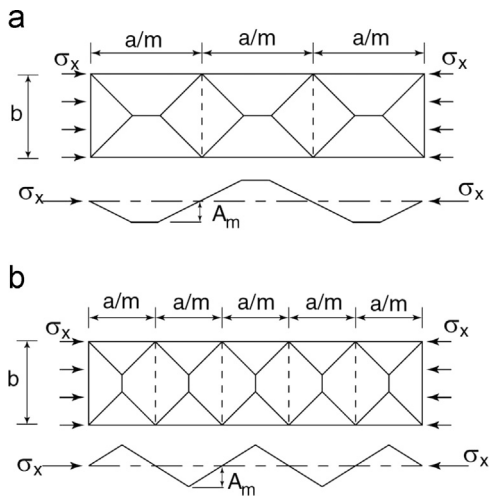

Fig. 7. Plastic mechanisms of plate under compression.

3.3. Relationship between average stress and deflection

3.3.1. Elastic range

The relationship between average stress and deflection in the elastic range is derived applying the elastic large deflection analysis (ELDA). The differential equation representing the compatibility condition of an initially deflected plate is expressed as

$$\nabla^4 F = E\left[\left(\frac{\partial^2 w}{\partial x \partial y}\right)^2 - \frac{\partial^2 w}{\partial x^2}\frac{\partial^2 w}{\partial y^2} - \left(\frac{\partial^2 w_0}{\partial x \partial y}\right)^2 + \frac{\partial^2 w_0}{\partial x^2}\frac{\partial^2 w_0}{\partial y^2}\right] \tag{11}$$

Fig. 6 shows a plate under longitudinal compression $\sigma = \sigma_x$.

Substituting the assumed initial deflection, Eq. (8), and total deflection, Eq. (9), into Eq. (11), the Airy's stress function is obtained in the following form

$$F = \frac{E(A^2 - A_0^2)}{32}\left[\alpha^2 \cos\frac{2m\pi x}{a} + \frac{1}{\alpha^2}\cos\frac{2\pi y}{b}\right] + \sigma \tag{12}$$

where

$$\alpha = \frac{a}{mb} \tag{13}$$

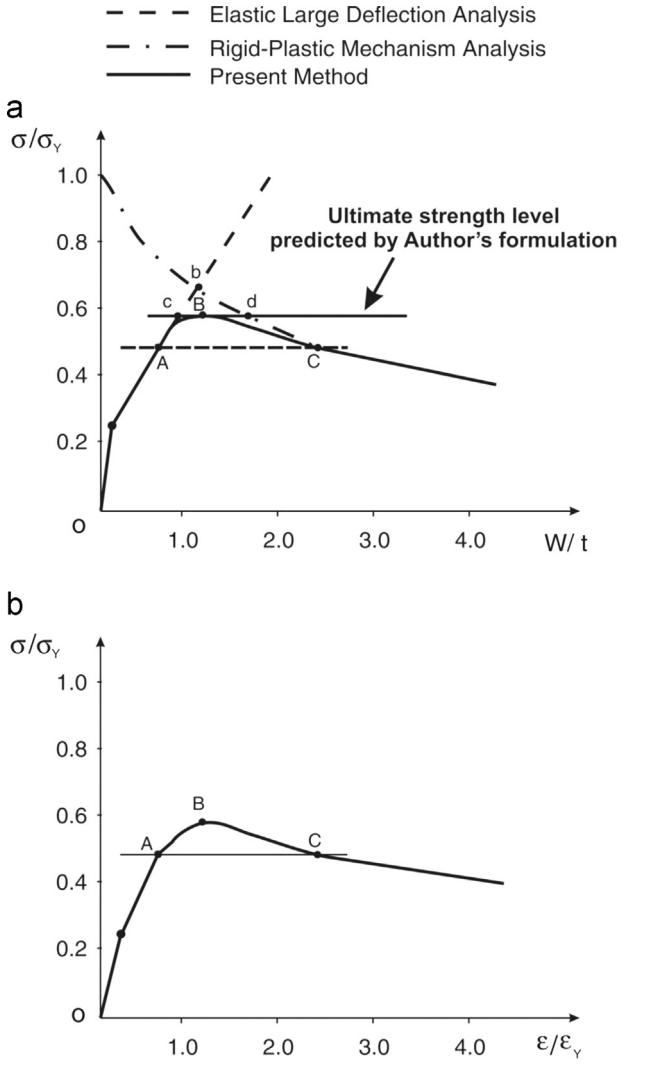

Fig. 8. Schematic representation of the present method for constructing the average stress-deflection and average stress–average strain relationships of the plate. (a) Average stress-deflection relationship. (b) Average stress-average stain relationship.

Having Airy's stress function, in-plane stress components are easily obtained as

$$\sigma_{xp}=\frac{\partial^2 F}{\partial y^2},\sigma_{yp}=\frac{\partial^2 F}{\partial x^2},\sigma_{xyp}=-\frac{\partial^2 F}{\partial x\partial y} \tag{14}$$

Applying the stress–strain relationships for the plane stress state, the corresponding in-plane strains are

$$\varepsilon_{xp}=\frac{1}{E}(\sigma_{xp}-\nu\sigma_{yp}),$$

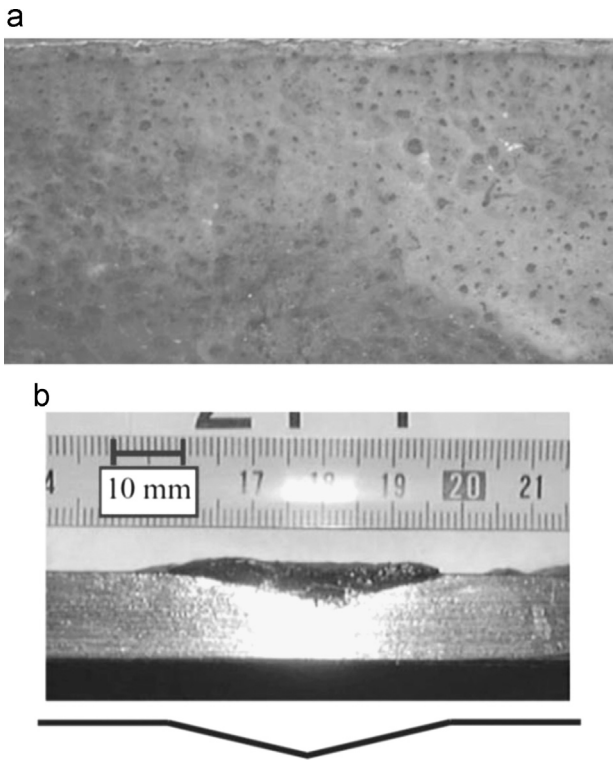

Fig. 9. Pitted web plate of the hold frame of a bulk carrier [10]. (a) Pitted surface. (b) Cross-sectional view.

$$\varepsilon_{yp}=\frac{1}{E}(\sigma_{yp}-\nu\sigma_{xp}),$$

$$\gamma_{xyp}=\frac{2(1+\nu)}{E}\tau_{xyp} \tag{15}$$

where ν is Poisson's ratio. On the other hand, the bending strain components are given as

$$\varepsilon_{xb}=-z\frac{\partial^2(w-w_0)}{\partial x^2},$$

$$\varepsilon_{yb}=-z\frac{\partial^2(w-w_0)}{\partial y^2},$$

$$\gamma_{xyb}=-2z\frac{\partial^2(w-w_0)}{\partial x\partial y} \tag{16}$$

While the corresponding bending stress components are

$$\sigma_{xb}=\frac{E}{1-\nu^2}(\varepsilon_{xb}+\nu\varepsilon_{yb}),$$

$$\sigma_{yb}=\frac{E}{1-\nu^2}(\varepsilon_{yb}+\nu\varepsilon_{xb}),$$

$$\tau_{xyb}=\frac{E}{2(1+\nu)}\gamma_{xyb} \tag{17}$$

The principle of virtual work is expressed as

$$\delta w_i=\delta w_e \tag{18}$$

where δw_i and δw_e are the internal and external virtual work done for a virtual deflection δA, respectively, and are expressed as

$$\delta w_i=\int_v[(\sigma_{xp}+\sigma_{xb})(\delta\varepsilon_{xp}+\delta\varepsilon_{xb})+(\sigma_{yp}+\sigma_{yb})(\delta\varepsilon_{yp}+\delta\varepsilon_{yb}) +(\tau_{xyp}+\tau_{xyb})(\delta\gamma_{xyp}+\delta\gamma_{xyb})]dv \tag{19}$$

and

$$\delta w_e=-\sigma bt\delta\overline{u} \tag{20}$$

Therefore, the average stress-deflection relationship is obtained as follows

$$\frac{\pi^2 E}{16b^2}\left(\frac{1}{\alpha^2}+\alpha^2\right)(A^2-A_0^2)+\sigma_{cr0}\left(1-\frac{A_0}{A}\right)-\sigma=0 \tag{21}$$

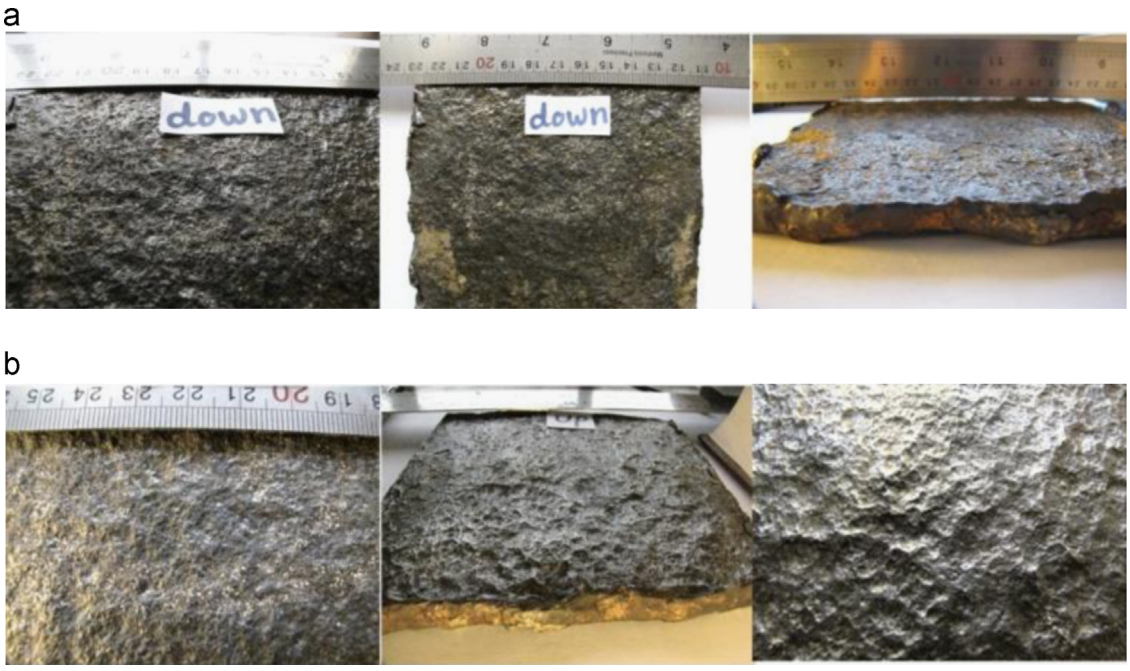

Fig. 10. Plate with general corrosion. (a) Lower surface. (b) Upper surface.

where

$$\sigma_{cr0}=\frac{\pi^2 t^2 E}{12(1-\nu^2)b^2}\left(\frac{1}{\alpha}+\alpha\right)^2 \tag{22}$$

σ_{cr0} is buckling strength of a simply-supported rectangular plate.

The incremental form of Eq. (21) is

$$\frac{\pi^2 E}{8b^2}\left(\frac{1}{\alpha^2}+\alpha^2\right)A\times\Delta A+\sigma_{cr0}\left(\frac{A_0}{A^2}\right)\times\Delta A-\Delta\sigma=0 \tag{23}$$

where

$$\Delta A=A_r-A_{r-1} \tag{24}$$

and

$$\Delta\sigma=\sigma_r-\sigma_{r-1} \tag{25}$$

3.3.2. Plastic range

With the increase in the applied end-shortening displacement, a plate undergoes buckling and yielding, and then attains its ultimate strength. After the ultimate strength, the compressive load decreases with the increase of the applied end-shortening displacement and deflection.

The average stress–plastic deflection relationship at the post-ultimate strength region is derived according to the rigid-plastic mechanism analysis (RPMA) assuming rigid-perfectly plastic material. Depending on the plate aspect ratio (a/b), two configurations of plastic mechanism may exist as illustrated in Fig. 7. For these mechanisms, the following relationships between the average stress and deflection coefficient are derived [8]

$$m_{45}+(1/\alpha-1)m_{90}/2=(2/\alpha-1)\overline{\sigma}\times\overline{A}\quad\text{for}\quad\alpha\le 1.0 \tag{26}$$

$$m_{45}+(\alpha-1)m_0/2=\overline{\sigma}\times\overline{A}\quad\text{for}\quad\alpha>1.0 \tag{27}$$

where $\overline{\sigma}=\sigma/\sigma_Y$, $\overline{A}=A/t$ and :

$$m_{90}=1-\overline{\sigma}^2 \tag{28}$$

$$m_0=2m_{90}/\sqrt{1+3m_{90}} \tag{29}$$

$$m_{45}=4m_{90}/\sqrt{1+15m_{90}} \tag{30}$$

3.4. Relationship between average stress and average strain

3.4.1. Elastic range

According to elastic large deflection analysis, the in-plane shortening in x-direction will become

$$\overline{u}=\frac{1}{b}\int_0^a\int_0^b\left[\varepsilon_x-\frac{1}{2}\left\{\left(\frac{\partial w}{\partial x}\right)^2-\left(\frac{\partial w_0}{\partial x}\right)^2\right\}\right]dydx=-\frac{a}{E}\sigma-\frac{m^2\pi^2}{8a^2}(A^2-A_0^2) \tag{31}$$

Dividing $\overline{u}$ by the plate length a, average stress–average strain relationship is derived as follows

$$\varepsilon=-\frac{1}{E}\sigma-\frac{m^2\pi^2}{8a^2}(A^2-A_0^2) \tag{32}$$

And its incremental form would be

$$\Delta\varepsilon=-\frac{1}{E}\Delta\sigma-\frac{m^2\pi^2}{4a^2}A\times\Delta A \tag{33}$$

where

$$\Delta\varepsilon=\varepsilon_r-\varepsilon_{r-1} \tag{34}$$

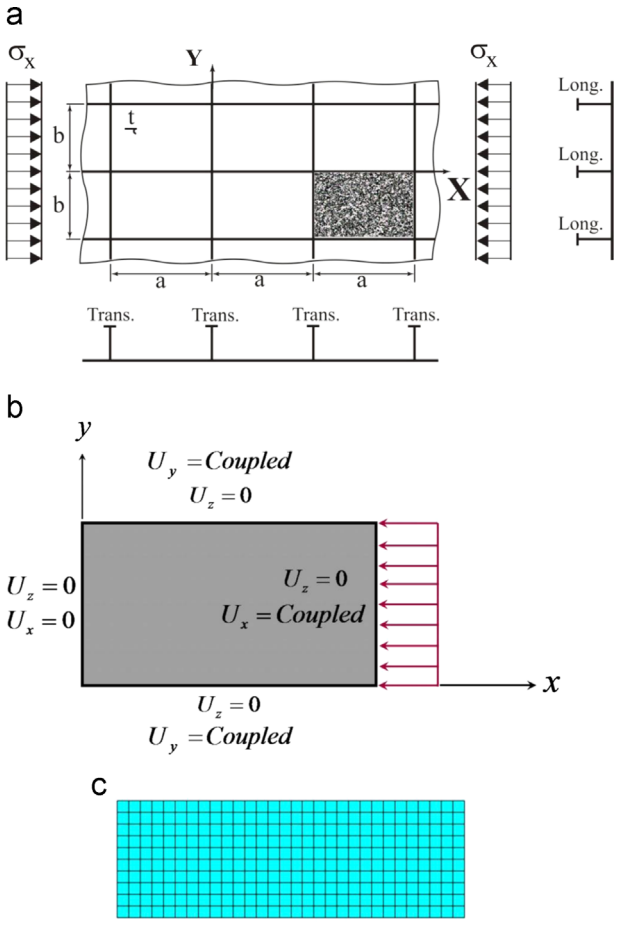

Fig. 11. (a) Extent of the model, (b) boundary and loading conditions, (c) finite element discretisation.

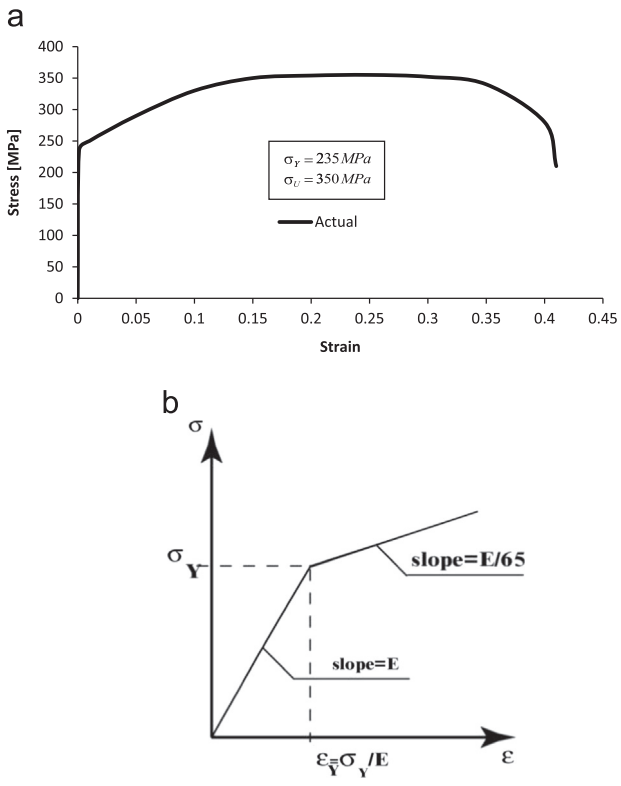

Fig. 12. Actual and applied stress–strain curves for normal strength (NS) steel. (a) Actual stress–strain curve. (b) Idealised bilinear model of stress–strain curve.

3.4.2. Plastic range

Based on rigid-plastic mechanism analysis, average stress–average strain relationship is derived as

$$\varepsilon = -\frac{1}{E}\sigma - \frac{2m^2}{a^2}(A^2 - A_0^2) \quad \text{for} \quad \alpha \le 1.0 \tag{35}$$

$$\varepsilon = -\frac{1}{E}\sigma - \frac{2m^2}{ab}(A^2 - A_0^2) \quad \text{for} \quad \alpha > 1.0 \tag{36}$$

Also, the incremental forms of above equations are

$$\Delta\varepsilon = -\frac{1}{E}\Delta\sigma - \frac{4m^2}{a^2}A \times \Delta A \quad \text{for} \quad \alpha \le 1.0 \tag{37}$$

$$\Delta\varepsilon = -\frac{1}{E}\Delta\sigma - \frac{4m^2}{ab}A \times \Delta A \quad \text{for} \quad \alpha > 1.0 \tag{38}$$

3.5. Procedure to obtain the average stress–deflection and average stress–average strain curves

The procedure to create the average stress–deflection and average stress–average strain curves is shown schematically in Fig. 8. The following steps are required to be done for obtaining these relationships

(1) Using Eq. (23) the average stress–deflection curve in the elastic range is drawn (dashed line in Fig. 8(a)).

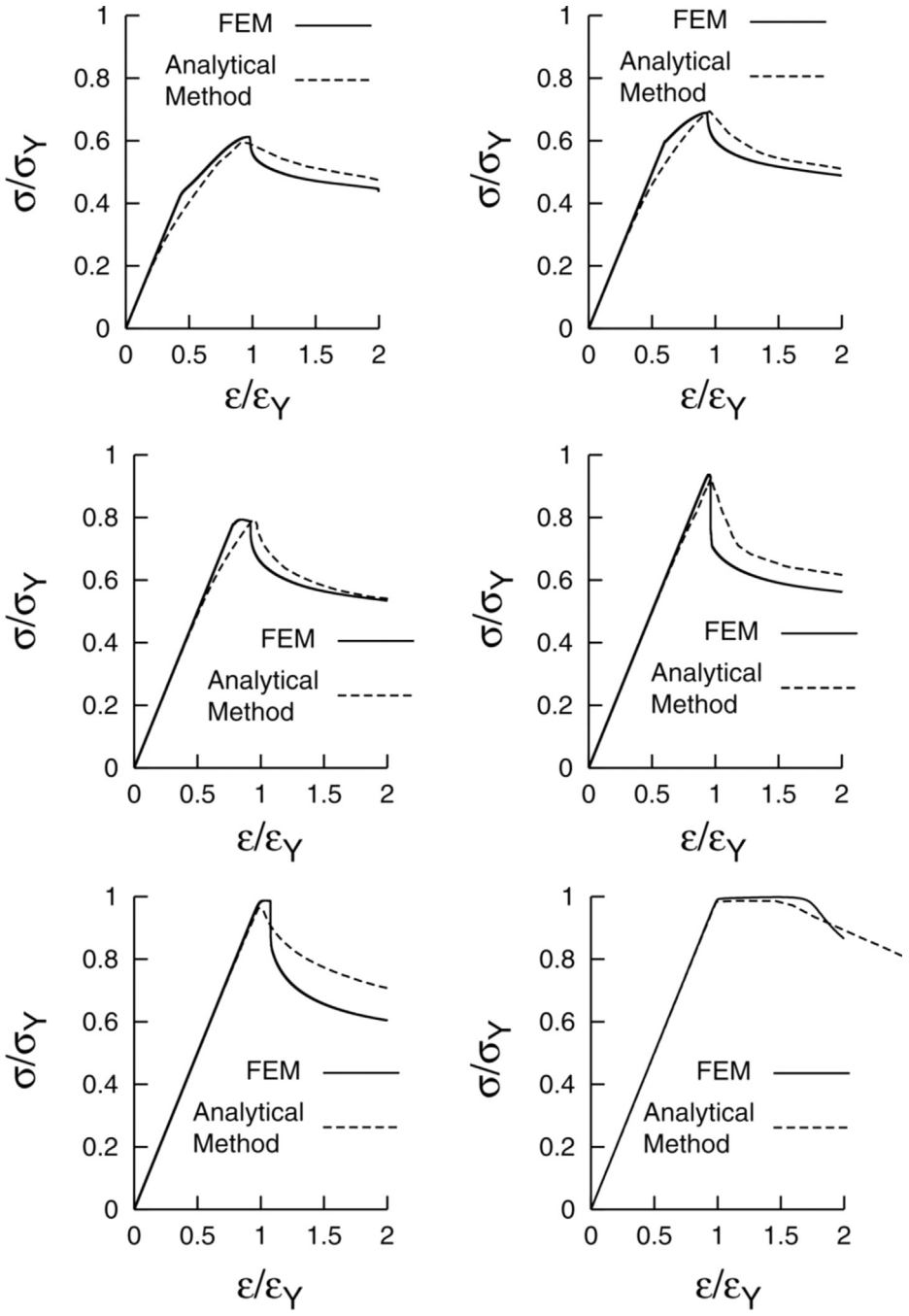

Fig. 13. Comparison between simulated average stress–average strain relationships with FEA results for the un-corroded plate (a=2400 mm, b=800 mm, made of NS steel).

(2) The average stress–deflection relationship is drawn in the plastic range based on Eqs. (26) and (27) (dotted-dashed line in Fig. 8(a)).
(3) The initial yielding stress level (point A) is determined by checking the stress state inside plate. A horizontal line AC is drawn at the initial yielding stress level.
(4) The ultimate compressive strength (σ_{Ult}) of the plate is accurately estimated by the second author's formula [9] as follows

$$\sigma_{Ult}/\sigma_Y = \begin{cases} 1.0 & \text{for } \beta \le 1.73 \\ 0.1+1.571/\beta & \text{for } \beta > 1.73 \end{cases} \quad (39)$$

(5) The stress level corresponding to the predicted ultimate strength is shown in Fig. 8(a) by the line cd. The deflection at the ultimate strength level for point B is determined by assuming $\overline{cB}/\overline{cd}$ as 1/3.
(6) Between points A and B, the deflection is approximated as

$$w = w_e + \overline{cB}\left(1-\sqrt{1-(\sigma-\sigma_A)^2/(\sigma_B-\sigma_A)^2}\right) \quad (40)$$

where w_e is the elastic deflection at the stress level σ.
(7) In the same manner, average stress-deflection relationship between points B and C is determined using the following equation

$$w = w_p + \overline{Bd}\left(1-\sqrt{1-(\sigma-\sigma_A)^2/(\sigma_B-\sigma_A)^2}\right) \quad (41)$$

where w_p is the plastic deflection at the stress level σ.
(8) In the same manner, the average stress–average strain curve (Fig. 8(b)) is obtained. To do that, Eq. (33) in the elastic range and Eqs. (37) and (38) in the plastic range are applied.

A special computer program was written in Fortran 77 language in order to implement the explained procedure *in an incremental way*.

4. Average stress–average strain relationship of both-sides randomly corroded plates

Corrosion in marine structures is mainly observed in two distinct types, namely, general corrosion and localised corrosion. As an example of localised corrosion, reference may be made to the corrosion of hold frames in way of cargo holds of bulk carriers which have coating such as tar epoxy paints, Fig. 9 [10]. Generally, pitting corrosion is defined as an extremely localised corrosive attack and sites of the corrosive attack are relatively small compared to the overall exposed surface [11]. In the case of localised corrosion observed on hold frames of bulk carriers, the sites of the corrosive attack, that is, pits are relatively large (up to about 50 mm in diameter).

General corrosion is the problem when the plate elements such as the hold frames of bulk carriers have no protective coating, Fig. 10. Both surfaces of the plate may be corroded, in a pattern like the sea waves spectrum, as shown in Fig. 10.

Based on the extensive results obtained by the authors [12,13], strength characteristics of a plate having random corrosion on it's both sides can be effectively assessed by considering an equivalent un-corroded plate with the equivalent thickness described by

$$t_{eq} = t-\mu-S \quad (42)$$

where t, μ and S are respectively representing the thickness of plate in un-corroded condition, mean corrosion depth and standard deviation of random thickness variations. Thus, for a both-sides randomly corroded plate of length a, breadth b and original thickness t in un-corroded condition with corrosion parameters of μ and S, firstly the equivalent thickness is to be determined using Eq. (42). Then the same procedure as explained in Section 3.5 is to be applied for another plate of the same length and breadth, but having an equivalent uniform thickness of t_{eq}.

5. Accuracy of the method

5.1. Un-corroded plates

The accuracy of the average stress–average strain relationships obtained by the analytical formulas and expressions derived above, are verified against those obtained applying FEA. Extent of plate model applied in FEA and its loading, meshing and boundary conditions have been shown in Fig. 11. In order to perform elastic–plastic analysis of plates, ANSYS code [14] has been used. Influences of both material and geometrical nonlinearities induced by yielding and large deflection are considered in the analyses.

Plates are modelled by SHELL181 elements with elastic–plastic large deflection solution option. SHELL181 is suitable for analyzing

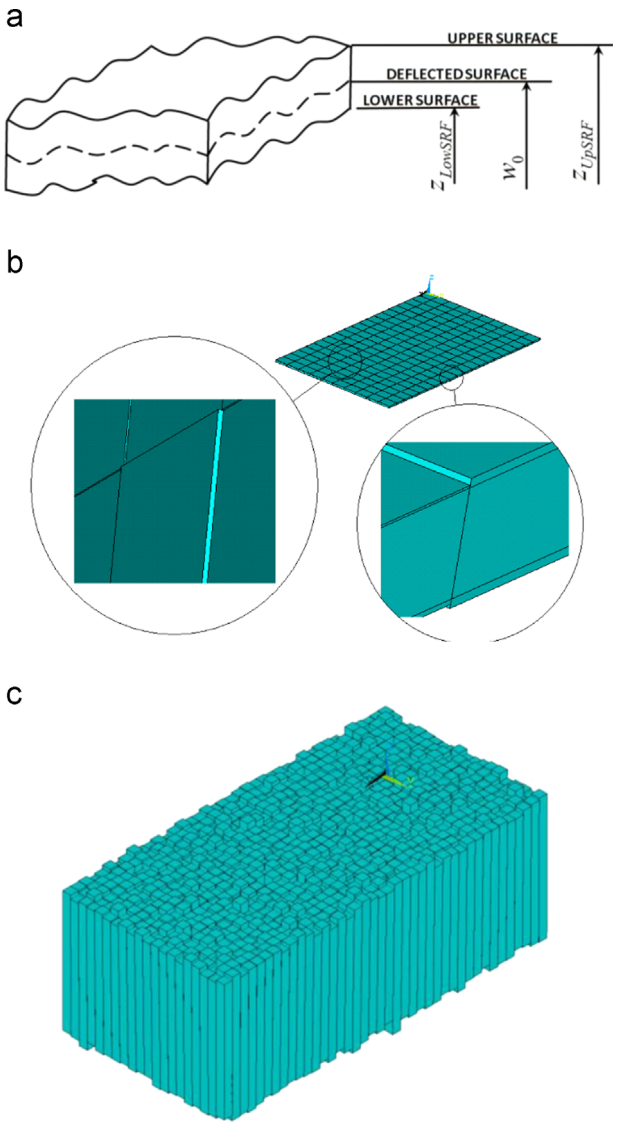

Fig. 14. Finite element analysis modeling details for general corrosion. (a) Different surfaces and relevant parameters. (b) Plate descretisation. (c) Perspective view of the randomly corroded plate with magnified thickness.

thin to moderately-thick shell structures. It is a 4-node element with six degrees of freedom at each node: translations in the x, y, and z directions, and rotations about the x, y, and z-axes. SHELL181 is well-suited for linear, large rotation, and/or large strain nonlinear applications. Change in shell thickness is accounted for in nonlinear analyses. In order to obtain reasonable results a number of sensitivity analyses were carried out to find out the optimum mesh density and proper values of nonlinear analysis options. A sample of finite element descretisations is represented in Fig. 11(c), which is relevant to a plate of aspect ratio equal to 3 with 30 and 10 numbers of mesh divisions in longitudinal and transverse directions, respectively.

Axial compression was simulated by an imposed displacement in longitudinal direction, applied in small enough increments to ensure that the analysis would closely follow the model load–response curve. The material was assumed of normal strength or so-called NS steel type, for which actual and applied stress–strain curves are shown in the Fig. 12. Yield stress (σ_Y), Young's modulus of elasticity (E) and Poisson's ratio (ν) of the material were respectively taken as 235 MPa, 205.8 GPa and 0.3.

It is evident that strain-hardening effect has some influence on the nonlinear behaviour of plates. The degree of such an influence is a function of many factors including plate slenderness. In this study, material behaviour for plate was modelled as a bi-linear elastic-plastic manner with strain-hardening rate of E/65, Fig. 12 (b). This value of strain-hardening rate was obtained through a large number of elastic–plastic large deflection analyses made by Khedmati [9]. w_0 and $w_{0\ \max}$ are obtained respectively according to Eqs. (4) and (6).

Some comparisons for a range of thin to thick plates are shown in Fig. 13. The plates have a length of 2400 mm, a breadth of 800 mm and a thickness of 10 mm to 20 mm. As can be seen from the results, good correlations are observed among them, although some more improvements are to be attempted in the future.

5.2. Both-sides randomly corroded plates

Randomly corroded surfaces were generated for both sides of the plate models. A special purpose computer code was written in FORTRAN90 language. Generation of randomly corroded surfaces was achieved using the features of the DRANDM function of FORTRAN90. There was one limitation in the generation process and it was standard deviation of the plate thicknesses at different nodes that was set to 0.23 mm, as investigated by Ohyagi [15]. Ohyagi corrosion model is adopted here as

$$d_w = 0.34 n_y \tag{43}$$

where n_y is the number of years of exposure and d_w is the uniform reduction in thickness in millimeters after n_y years of exposure. Eq. (43) represents a linear corrosion model and is used here in as an example. It is obvious that the effectiveness of simulation procedure explained in this paper is independent of the corrosion model.

Finally the z-coordinate of upper and lower surfaces of the plate can be defined as, Fig. 14(a)

$$z_{LowSRF} = w_0 - \frac{t-d_w}{2} - r_1 \quad , \quad z_{UpSRF} = w_0 + \frac{t-d_w}{2} + r_2 \tag{44}$$

where

$$t_p = z_{UpSRF} - z_{LowSRF} = t - d_w + r_1 + r_2 \tag{45}$$

and also r_1 and r_2 are the random numbers, corresponding to the

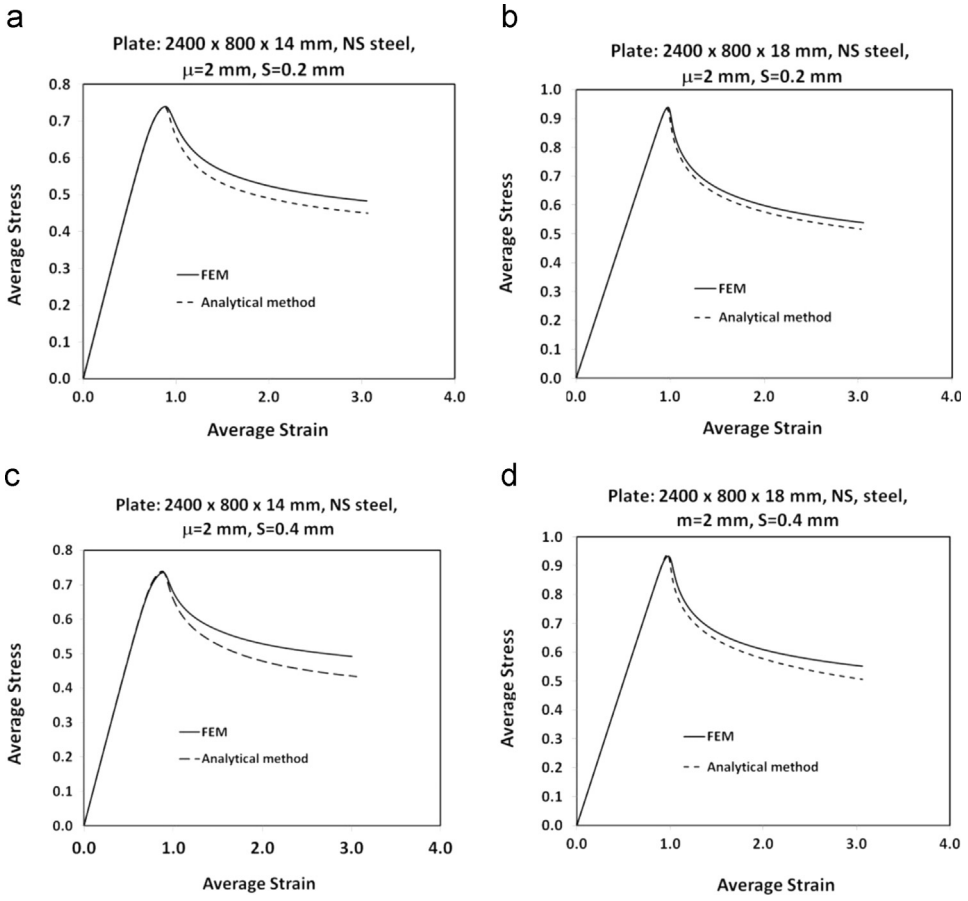

Fig. 15. Comparison between simulated average stress–average strain relationships with FEA results for the corroded plate.

random thickness variation of the plate surfaces, produced by DRANDM function. Again w_0 and $w_{0\,max}$ are obtained respectively according to Eqs. (4) and (6).

There are several finite element techniques available to model uniform corrosion. The easiest way is to reduce the thickness of the plate in surface, carry out buckling analysis to get the buckled shape of plate with uniform corrosion and finally to perform nonlinear finite element control to get the ultimate strength of plate by using stress versus strain relationship. Khedmati and Karimi [16] modelled corroded plate with 3-D 20-node structural solid element but this method also cannot represent the real situation and easily tends to fail to converge during nonlinear control based on author's experience.

Fig. 14(b) represents modelling details in finite element analysis, while Fig. 14(c) shows a magnified view of the plate with surfaces simulating random corrosion. The same elements in ANSYS code were used in descretisation of the corroded plate models.

Some comparisons between simulated average stress–average strain relationships with FEA results for the corroded plate models are shown in Fig. 15. Again good correlation is observed between two groups of FEM results and analytical ones.

6. Conclusions

A simple method for simulation of the average stress–average strain relationships of plates under the action of longitudinal axial compression is developed. The features of the method are:

- The results of elastic large deflection analysis and rigid-plastic mechanism analysis are combined together in derivation of the average stress–average strain relationship of the plates. The influences of buckling and plastic deformations are accounted for in the formulations.
- The procedure is capable of simulating the average stress–average strain relationship for un-corroded as well as both-sides randomly corroded plates.
- The results show that the explained method is a simple and relatively accurate and can be applied effectively in the ultimate strength evaluation of ship hull girders and other box-like structures.

References

[1] Smith CS. Influence of local compressive failure on ultimate longitudinal strength of a ship's hull. Tokyo: PRADS; 1977.
[2] Smith CS. Structural redundancy and damage tolerance in relation to ultimate ship hull strength. In: International symposium on the role of design, inspection and redundancy in marine structural reliability, Williamsburg, 1983.
[3] Yao T, Fujikubo M, Yanagihara D Varghese B. Influences of welding imperfections on buckling/ultimate strength of ship bottom plating subjected to combined bi-axial & lateral pressure. In: Thin-walled structures, second international conference on thin-walled structures, Elsevier, 1998:425–432.
[4] Smith CS. Imperfection effects and design tolerances in ships and offshore structures. Trans Inst Eng Shipbuilders Scotland 1981;124:37–46.
[5] Ueda Y, Yao T. The influence of complex initial deflection on the behaviour and ultimate strength of rectangular plates in compression. J Const Steel Res 1985;5:265–302.
[6] Yao T, Nikolov PI, Miyagawa Y. Influence of welding imperfections on stiffness of rectangular plates under thrust. In: Karlsson K, Lindgren LE, Jonsson M, editors. In: Proceedings of IUTAM Sump on mechanical effects of welding. Springer-Verlag; 1992. p. 261–8.
[7] Smith CS, Davidson PC, Chapman JC, Dowling PJ. Strength and stiffness of ships plating under in-plane compression and tension. Trans RINA 1987;137:277–96.
[8] Okada H, Oshima K, Fukumoto Y. Compressive strength of long rectangular plates under hydrostatic pressure. J Soc Naval Arch Jpn 1979;146:270–80 (in Japanese).
[9] Khedmati MR. Ultimate strength of ship structural members and systems considering local pressure effects. (Dr. Eng. dissertation (Supervisors: Tetsuya Yao and Masahiko Fujikubo). Grad. School of Eng., Hiroshima University; 2000 (Oct.).
[10] Nakai T, Matsushita H, Yamamoto N. Effect of pitting corrosion on local strength of hold frames of bulk carriers (1st report). Mar Struct 2004;17:403–32.
[11] ASM International Corrosion. ASM Handbook. 2001, Vol. 13.
[12] Nouri ZHME. Assessment of effective thickness for practical evaluation of ultimate strength and post-buckling behaviour of both-sides randomly corroded steel plates under uniaxial compression. (Interim progress report of PhD thesis (Supervisor: Mohammad Reza Khedmati). Faculty of Marine Technology, Amirkabir University of Technology; 2010 (January).
[13] Roshanali MM. Strength of plates with randomly distributed corrosion wastage under uniaxial compression, MSc thesis (Supervisor: Mohammad Reza Khedmati), Faculty of Marine Technology, Amirkabir University of Technology, February 2010.
[14] ANSYS 11.0 reference manual, ANSYS Inc. 2008.
[15] Ohyagi M. Statistical survey on wear of ship's structural members. Tokyo: NK Technical Bulletin; 1987.
[16] Khedmati MR, Karimi AR. Ultimate compressive strength of plate elements with randomly distributed corrosion wastage. In: Topping BHV, Montero G, Montenegro R, editors. In: Proceeding of the eight international conference on computational structural technology. Civil-Comp Press; 2006.